Supplementary Information (SI) for Journal of Materials Chemistry C.

SUPPLEMENTARY INFORMATION

High Performance $BaTiO_3$–$SrTiO_3$ Ceramics with Refined Microstructure Obtained by Current-Controlled Reactive Flash Sintering of Mixed Powders

Samuel López-Blanco,[a] Xavier Vendrell,[b] Nerea Morante,[b] and Jose E. García[a]

[a] Department of Physics, Universitat Politècnica de Catalunya – BarcelonaTech, 08034 Barcelona, Spain.

[b] Department of Inorganic and Organic Chemistry, Universitat de Barcelona, 08028 Barcelona, Spain.

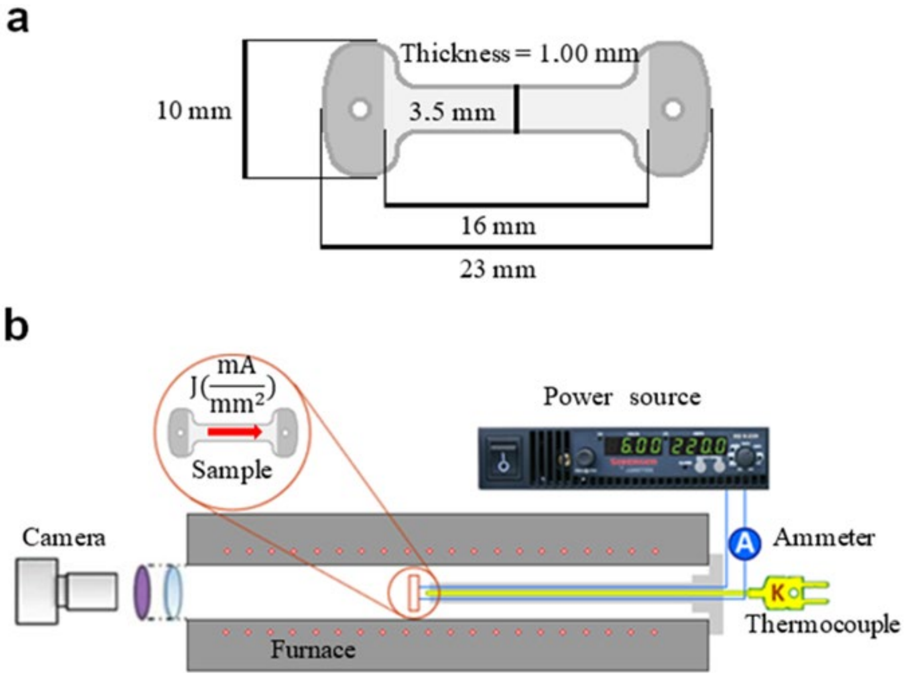

Figure S1. (a) Dimensions of a green sample after uniaxial pressing. Darker regions in the sample represent platinum painted electrodes. (b) Flash sintering experimental setup scheme. The sample is hanged inside the furnace using platinum wires. A homemade software controls the programmable DC power supply (Ametek XG 600-2.6), keeping its operation mode in current control at all times.

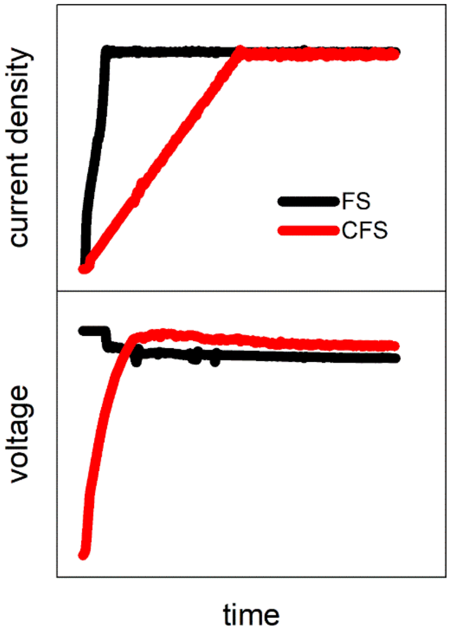

Figure S2. Comparison between the current profile of a conventional flash sintering (FS) experiment and a ramped current-controlled flash sintering (CFS) experiment. Experiments are performed at a given temperature that depends on the electric field necessary to maintain the current density. Flash sintered samples are held under electric field control prior to reaching the preset maximum current density, instant at which the power supply switches to current control. The samples are therefore let to flash freely and undergo a sharp rise in their current density. Current-controlled flash sintered samples are held exclusively under current control, inducing a slow increase in their current density during flash, thereby avoiding the current spike.

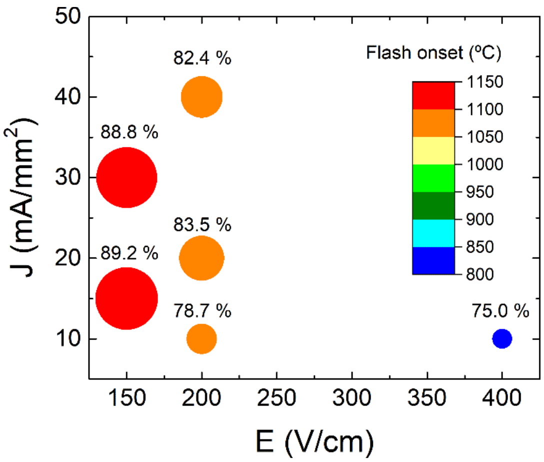

Figure S3: Density (%) and onset temperature (°C) of conventional reactive flash sintering experiments of $BaTiO_3$–$SrTiO_3$ ceramics performed under different thermo-electrical conditions. Onset temperature is shown with a coloured code while the circles size represents the obtained density.

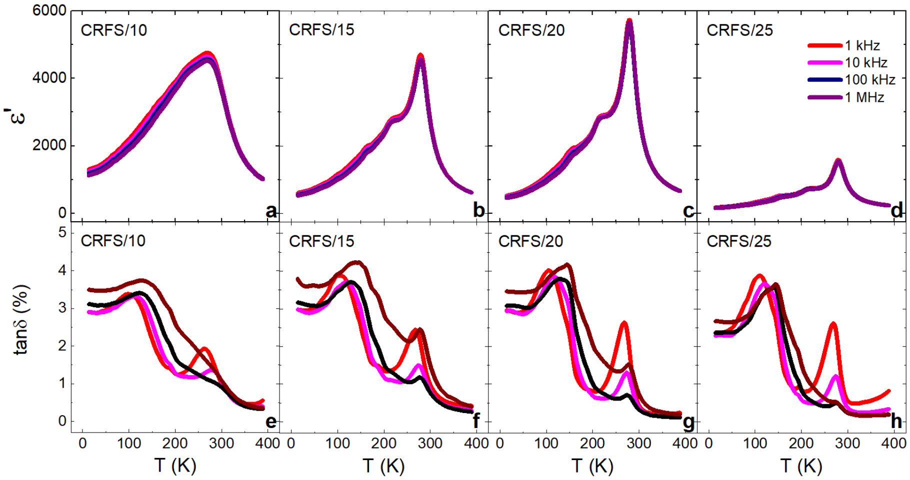

Figure S4. Temperature dependent of (a-d) real permittivity, ε′, and (e-h) dielectric losses, tan δ, of the representative CRF-sintered $Ba_{0.6}Sr_{0.4}TiO_3$ samples at several frequencies.

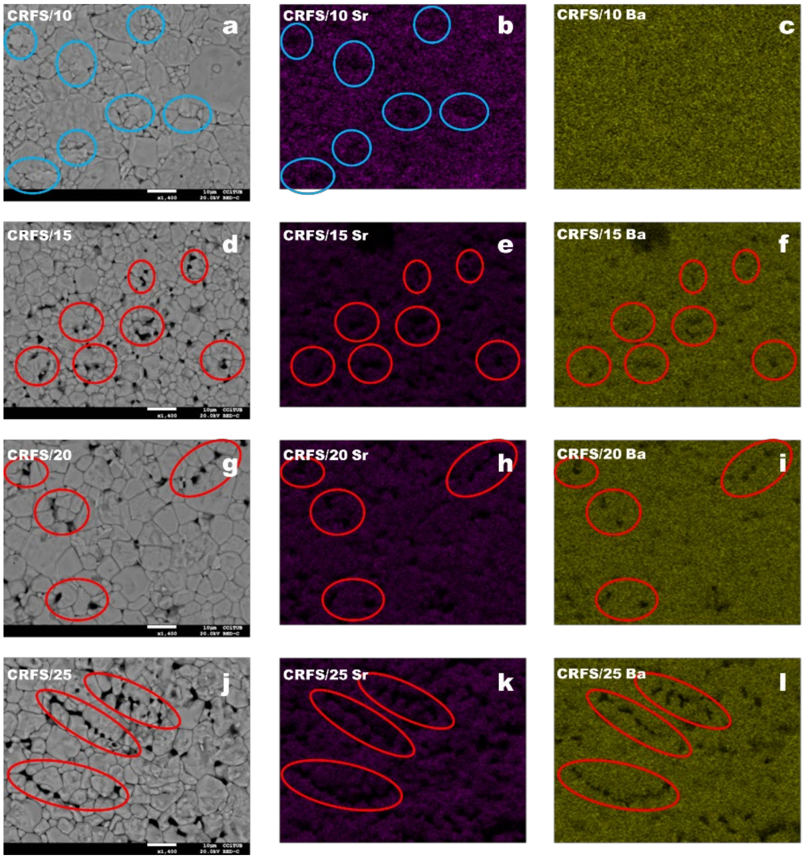

Figure S5. EDX mapping of CRF-sintered $Ba_{0.6}Sr_{0.4}TiO_3$ samples. The CRFS/10 sample shows Sr deficiency in regions with smaller grains, while Ba concentration remains evenly distributed (a-c). The remaining samples display a homogeneous distribution of both elements (d-l), with Sr deficiency observed only near the pores, where Ba is also lacking. The bimodal microstructure of the CRFS/10 sample appears to result from the formation of selective flash sintering paths along $SrTiO_3$-rich regions.

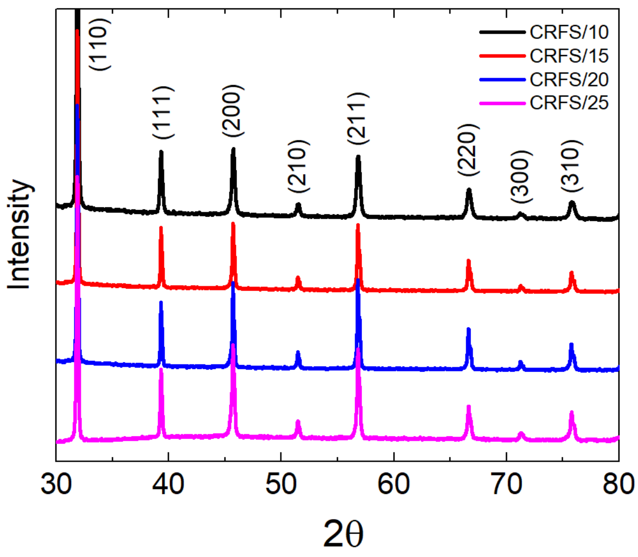

Figure S6. Normalized X-ray diffraction spectra of the representative CRF-sintered $Ba_{0.6}Sr_{0.4}TiO_3$ samples. All samples exhibit similar pattern profiles, corresponding to a cubic perovskite phase with no visible spurious phases. The measurement system used does not filter the $CuK\alpha_2$ signal. Furthermore, the CRF-sintered samples are considered too small for the device, leading to a convolution of the CuKα signals. Nevertheless, the peak widths remain consistent across all samples, confirming the presence of the cubic perovskite structure.

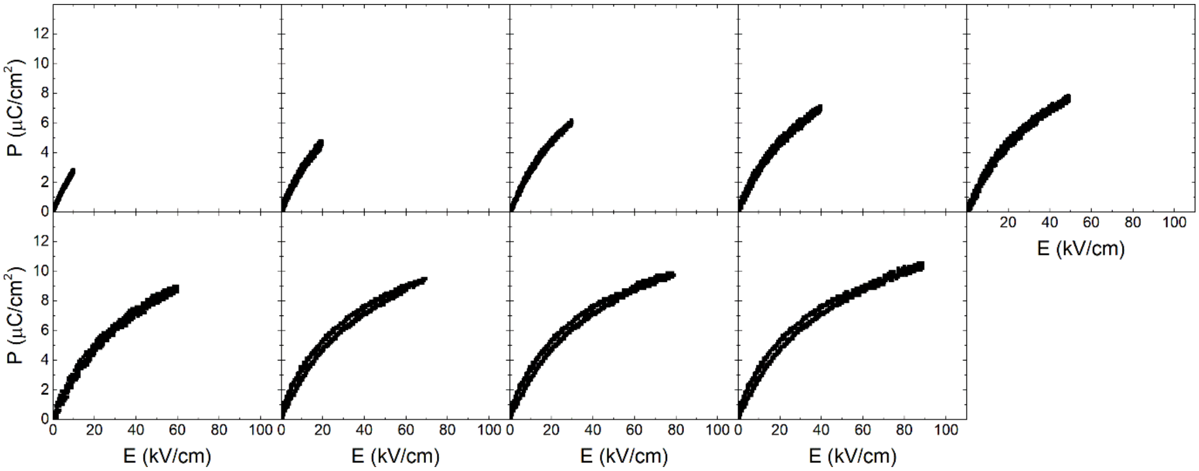

Figure S7. Unipolar P-E loops at different electric fields of CRF-sintered $Ba_{0.6}Sr_{0.4}TiO_3$ sample obtained at a current density of 15 mA/mm^2 (CRFS/15).

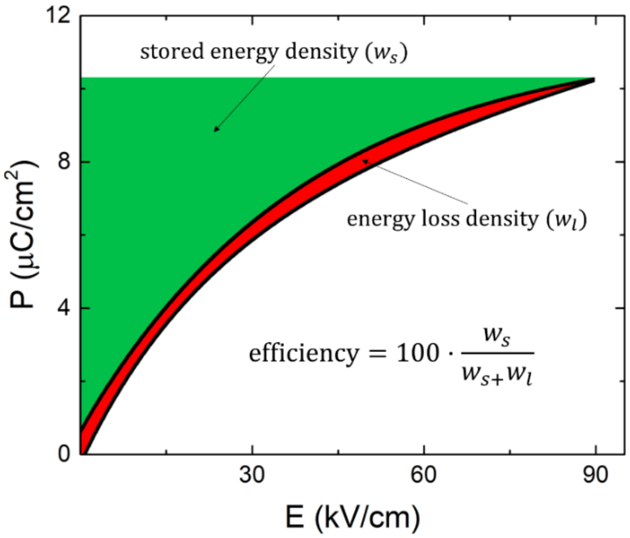

Figure S8. Unipolar P-E loop at 90 kV/cm of CRF-sintered $Ba_{0.6}Sr_{0.4}TiO_3$ sample obtained at a current density of 15 mA/mm^2 (CRFS/15). Storage and loss energy densities are shown in green and red, respectively.

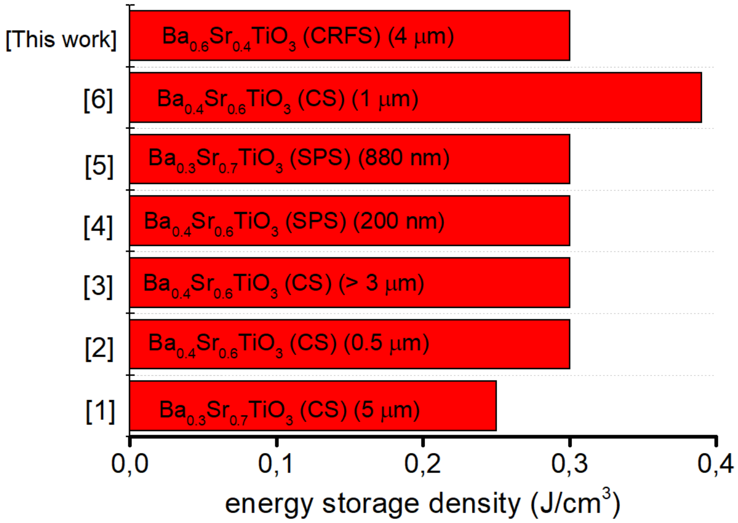

Figure S9. Reported values of energy storage density for some $Ba_{1-x}Sr_xTiO_3$ materials. The values are estimate for an applied electric field of 80-90 kV/cm. The specific composition, the reported medium grain size, and the employed sintering route (i.e., CS: conventional sintering, SPS: spark plasma sintering) are shown inside each bar.

[1] Ceram. Int. 35, 2069–2075 (2009).
[2] J. Eur. Ceram. Soc. 34, 1209–1217 (2014).
[3] Ceram. Int. 41, 8252–8256 (2015).
[4] J. Alloys Compd. 701, 439-446 (2017).
[5] J. Eur. Ceram. Soc. 37, 2099–2104 (2017).
[6] J. Alloys Compd. 617, 399–403 (2014).

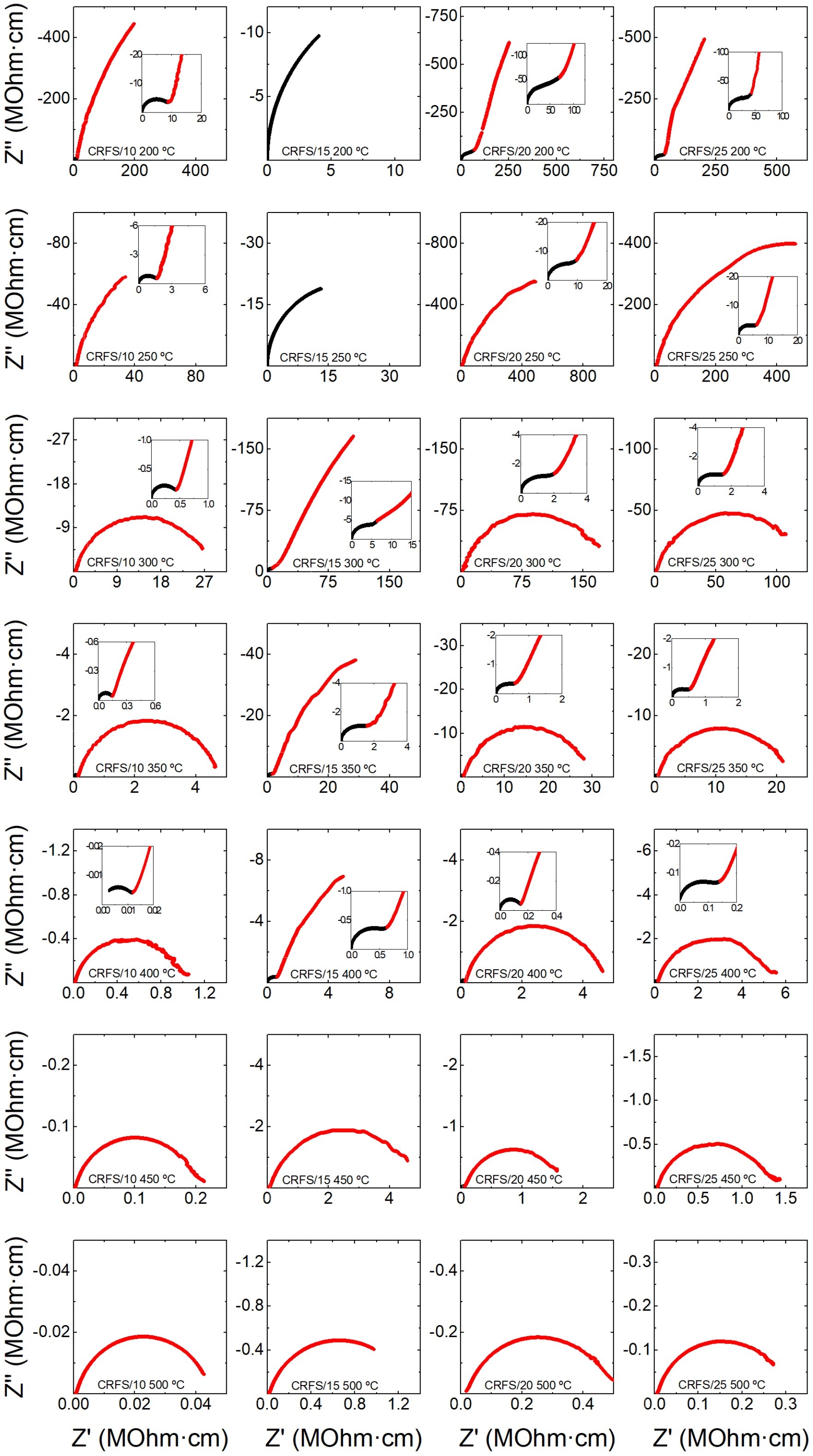

Figure S10. Z* plots at different temperatures for CRF-sintered $Ba_{0.6}Sr_{0.4}TiO_3$ samples. Colors indicate bulk (black) and grain boundary (red) contributions. Bulk and grain boundary AC resistances can be derived from the intercept of the high and low frequency arcs or distorted semicircles on the real (Z') axis.